RSC Advances

ROYAL SOCIETY OF CHEMISTRY

www.rsc.org/advances

RSC Advances

ARTICLE

Novel hybrid membranes by incorporating SiO_2 nanoparticles using in-situ microemulsion polymerization: preparation, characterization and enhancement on the performance for CO_2/N_2†

Received 00th January 20xx,
Accepted 00th January 20xx

DOI: 10.1039/x0xx00000x

www.rsc.org/

Ting Wang,[a] Cheng Cheng, [a] Jiang-nan Shen,[b] Li-guang Wu,[a*] Bart Van der Bruggen[c] and Chun-ying Dong[a]

SiO_2 nanoparticles were synthesized in a water-in-oil microemulsion using triblock copolymer as the surfactant and methyl methacrylate as the oil phase. Then, SiO_2/poly(methyl methacrylate) (PMMA) hybrid membranes were prepared by in situ microemulsion polymerization. The separation of CO_2/N_2 gas mixtures was studied using these novel membranes. Both the gas permeability and separation performance of the hybrid membranes first increased and then decreased with SiO_2 content. When the SiO_2 content was 4.0 wt%, the CO_2 permeability and permeability selectivity of the membranes for CO_2/N_2 gas mixtures were both at a maximum. For comparison, two commercially available SiO_2 nanoparticles were also used to synthesize SiO_2/PMMA membranes by solution polymerization. The particle size of SiO_2 in the microemulsion was close to the two commercially available SiO_2 nanoparticles. The SiO_2 nanoparticles formed in microemulsion distributed more homogeneously in the membranes than the commercially available nanoparticles because of protection by water droplets. Moreover, the SiO_2 nanoparticles formed in the water droplets and reverse microemulsion had a strong polar surface. Therefore, the SiO_2/PMMA hybrid membrane formed by the in situ microemulsion polymerization had better performance than the hybrid membranes made with commercially available SiO_2 nanoparticles.

Introduction

Global warming due to emission of greenhouse gases from fossil fuels is one of the most important environmental global issues [1-3]. The efficient and economical separation of CO_2 greenhouse gas from flue gas and low-grade natural gas has received significant attention as an important technology for the protection of the environment [4, 5]. Polymer membranes are attractive for this purpose because they are inexpensive, low energy intensive, and require no phase transfer. Currently, the selectivity of CO_2 to N_2 at room temperature obtained with typical membranes [6–8] is not high enough. Over the last decade, membrane performance for gas separation has steadily improved. Organic–inorganic hybrid membranes have emerged as attractive materials because of their desirable organic and inorganic properties [9–11].

Incorporating inorganic nanoparticles into the polymeric matrix can not only disrupt the polymer chain packing [9-11], but also form the defects at the interface polymer-filler, thus improving the membrane performance [12, 13]. Several studies have indicated that such hybrid membranes substantially increased the permeability without deteriorating the selectivity [9–11]. Nonporous silica (SiO_2) nanoparticles are of interest because of their excellent properties including large surface area, a three-dimensional structure with highly open spaces, and facile surface functionalization [14, 15]. Kusakabe et al. [16] reported that the addition of inorganic SiO_2

[a] School of Environmental Science and Engineering, Zhejiang Gongshang University, Hangzhou, 310012, China. E-mail: wulg64@hotmail.com
[b] Center for Membrane and Water Science, Ocean College, Zhejiang University of Technology, Hangzhou 310014, China.
[c] Department of Chemical Engineering, Process Engineering for Sustainable Systems (ProcESS), KU Leuven, W. de Croylaan 46, B-3001 Leuven, Belgium.

† Electronic Supplementary Information (ESI) available: The scheme on the preparation of SiO_2/PMMA by in-situ microemulsion polymerization was listed in Scheme S1. Experimental setup for gas permeation measurements, TEM micrographs of SiO_2 nanoparticles in the microemulsion at SiO_2 content of 1.0 wt% SEM micrographs of the surface of SiO_2/PMMA hybrid membranes at SiO_2 content of 1.0 wt%, Effect of feed pressure on the CO_2 permeability of different SiO_2/PMMA membranes, Effect of feed pressure on the CO_2 permeability (Gas mixture, volume ratio of CO_2/N_2 are 9:1), Effect of feed pressure on the CO_2 permeability (Gas mixture, volume ratio of CO_2/N_2 are 5:5), The zeta potential values and water contact angles of different hybrid membranes containing different SiO_2 nanoparticles were listed in Figure S1~S8. See DOI: 10.1039/x0xx00000x

nanoparticles into a polyimide matrix increased the CO_2 permeability by a factor 10. The permeability and selectivity increased by adding nanostructured/fumed silica to several glassy, high free volume polymers [17, 18].

Similar to most nanocomposite membranes, the performance of these membranes is determined by the morphology of the inorganic nanoparticles including particle size and distribution in the membranes. Hybrid membranes containing small (1–20 nm) inorganic particles have a better behavior than those containing large (>50 nm) inorganic particles because smaller particles have a larger surface area and allow extensive organic/inorganic interactions [19]. Several methods have been reported to overcome the aggregation of nanoparticles and improve their distribution in the membranes [19–22]. One of the most promising methods is in situ microemulsion polymerization [23]. Based on this method, we first used a polymerizable monomer (methyl methacrylate) as the oil phase to form the water-in-oil (W/O) microemulsion as well as AgCl nanoparticles [24–26]. Then, hybrid membranes containing the nanoparticles were synthesized after monomer polymerization. In previous studies [24–26], poly(methyl methacrylate) (PMMA) hybrid membranes containing well distributed AgCl nanoparticles were prepared via in situ microemulsion polymerization. The hybrid membranes showed a high separation performance for benzene because of the small size and excellent distribution of the AgCl particles in the membranes. During this preparation process, the morphology of the AgCl nanoparticles could be regulated by changing the reaction conditions such as the type of surfactant, surfactant concentration, and reactant concentration. These changes consequently resulted in different membrane performance.

Based on the results of our previous study [26, 27], we applied the in situ microemulsion polymerization method to synthesize PMMA hybrid membranes incorporating SiO_2 nanoparticles for CO_2 separation. Then, PMMA hybrid membranes containing SiO_2 with different contents were prepared by in situ microemulsion polymerization, and the effect of SiO_2 content on the separation performance of the hybrid membranes was investigated. In addition, two commercially available SiO_2 nanoparticles were used to prepare SiO_2/PMMA membranes by solution polymerization for comparison.

Experimental

Materials

The poly(ethylene oxide) (PEO)–poly(propylene oxide) (PPO)–PEO triblock copolymer Pluronic F127—with a molecular weight of 12,600 and a PEO content of 70 wt%—was obtained from Sigma-Aldrich (USA). Tetraethylorthosilicate (TEOS), 2-azobisisobutyronitrile (AIBN), and ammonia were obtained from Shanghai Reagent Factory (Shanghai, China). Methyl methacrylate (MMA) was obtained from Chengdu Chemical Reagent Factory (Chengdu, China) and purified by vacuum distillation. Hydrophilic SiO_2 Aerosil 200 (diameter, 12 nm; specific surface area, 200 m^2/g) and hydrophobic SiO_2 Aerosil R972 (diameter, 16 nm; specific surface area, 130 m^2/g) were obtained from Degussa (Germany). The polysulfone film used in this manuscript with a molecular weight cutoff of 20,000 was obtained from Hangzhou Development Center of Water Treatment Technology (Hangzhou, China).

Preparation of SiO_2/PMMA hybrid membranes

Preparation of SiO_2/PMMA hybrid membranes by in situ microemulsion polymerization. The microemulsions were prepared by mixing deionized water(100 μL), F127(1.4 g), and MMA(27 mL, 25.49 g) in a flask. The resulting mixture was placed in an ultrasonic bath at 40°C until a homogeneous, transparent, and fluid isotropic phase was obtained (as shown in Scheme S1, Supporting Information). TEOS (Table 1) was added to the microemulsion and hydrolyzed in the water droplets via ultrasonication. After reaction for 5 h at 40 °C, the reverse microemulsion containing the SiO_2 nanoparticles was generated.

Table 1. Added amounts of TEOS in preparation and SiO_2 content in hybrid membrane after polymerization

Added amounts of TEOS /g	0.935	1.870	2.805	3.740	4.675
SiO_2 content in hybrid membranes after polymerization (Mass percentage) /wt%	1.0	2.0	3.0	4.0	5.0

The initiator (AIBN) was added to the MMA microemulsions containing SiO_2 nanoparticles. The microemulsions were then stirred to start the polymerization at 60-65 °C. After mixing for 2 h (when the viscosity of the reaction mixture reached ~300 mPa·s)

the resulting solution was used to coat a polysulfone film (molecular weight cut-off = 20,000). The SiO_2/PMMA hybrid membranes on the polysulfone film were then obtained by continuing the reaction for another 12 h at 60-65 °C and denoted as M-SiO_2/PMMA.

Preparation of SiO_2/PMMA by solution polymerization. Hydrophilic or hydrophobic SiO_2 from Degussa were added to 30 mL of MMA (28.32 g). The resulting mixture was stirred for ~5 h and then placed in a fixed frequency ultrasonic bath for ~1 h to improve the SiO_2 dispersion in the MMA and achieve a homogeneous solution. The AIBN was added to this homogeneous solution with stirring at 60-65°C to initiate the polymerization. When the viscosity of the reaction mixture reached ~300 mPa·s, the reaction solution was used to coat a polysulfone film (molecular weight cut-off = 20,000). SiO_2/PMMA hybrid membranes with different SiO_2 contents on the polysulfone film were obtained by continuing the polymerization reaction for another 12 h at 60-65 °C. The thickness of the top polymer membrane was measured at about 15 μm by scanning electron microscopy (SEM).

Characterization

The growth of SiO_2 nanoparticles in the microemulsion was measured by UV-visible absorption spectroscopy using a UV-2450 spectrophotometer (Shimadzu Co., Ltd., Japan). One drop of an ultrasonic-mixed, dilute alcohol suspension of the SiO_2 nanoparticles was placed on a carbon-coated grid. After an evaporation of the solvent, the morphology of the SiO_2 nanoparticles was characterized with a JEM-1230 transmission electron microscope (TEM) (Jeol Co., Ltd., Japan). The surface morphology of membranes containing the SiO_2 nanoparticles were analyzed using an S-4700 scanning electron microscope (SEM) (Hitachi Co., Ltd., Japan). The structure of different SiO_2 nanoparticles was characterized by Fourier transform infrared (FTIR, Nexus-670, Nicolet Co.). The thermal stability of the hybrid membrane was determined by differential scanning calorimetry (DSC, Perkin-Elmer DSC7) from 25 °C to 300 °C under N_2 at a heating rate of 10 °C·min^{-1}. The static water contact angles of hybrid membranes were determined using a contact ang5.e goniometer (SL200B, Kono Co., Ltd.). The zeta potential measurements of the hybrid membranes were conducted using a solid surface potentiometer (SurPASS, Anton Paar Co., Ltd.).

Gas permeability measurements

The permeability and separation properties of the membranes were examined with a steady-state measurement method using a CO_2/N_2 gas mixture (volume ratio, 1:9) and pure gas (CO_2 and N_2) at 303 K and feed pressure of 0.105 MPa and atmospheric pressure on the permeate side. Feed and permeate side gas flow rate was 2 mL·s^{-1} (Experimental setup is shown in Figure S1, SI). The retentate compositions were measured using a gas chromatograph. The pressure on each side of the membrane was independently measured and controlled. The membrane module temperature was controlled using a thermostatic water bath. The permeability coefficient was calculated in triplicates for each membrane. The error in the absolute values of the permeability coefficients was about ±5%.

The gas permeability and permeability selectivity for CO_2/N_2 were calculated by the following equations [27-29]:

$$P_A = \frac{N_A l}{p_2 - p_1} \quad (1)$$

where N_A is the steady state gas flux through the film, l is the film thickness, and p_2 and p_1 are the upstream and downstream partial pressures of gas A, respectively.

The CO_2/N_2 selectivity is calculated by the following equation::

$$\alpha_{CO_2/N_2} = \frac{P_{CO_2}}{P_{N_2}} \quad (2)$$

Since the permeate side is maintained at ambient pressure, the mixed-gas separation factor could also be calculated by Eq. (2).

In addition, feed pressure test using a CO_2/N_2 gas mixture (volume ratio, 1:9) and pure CO_2 gas was carried out from 0.105 MPa to 1.05 Mpa to acquire more comprehensive information about membrane separation performance.

Results and discussion

Generation of SiO_2 nanoparticles in the reverse microemulsion

The formation of SiO_2 nanoparticles in the reverse microemulsion was characterized by UV-visible spectroscopy (Fig. 1A). The UV-visible spectra of the two commercially available SiO_2 nanoparticles dispersed in MMA (30 mL, 28.32 g) are listed in Fig. 2B for comparison (containing 3.0 wt% of SiO_2). The sample has an absorption peak at λ_{max} ~295 nm and is the characteristic absorbance of SiO_2 nanoparticles (Fig. 1B). This characteristic absorption appears after 1 h of reaction for the reverse microemulsion sample. Therefore, the SiO_2 nanoparticles began to form in the microemulsion after 1 h. The characteristic absorption peak of SiO_2 becomes stronger, and the width of the peak changed slightly within 5 h indicating that the number of SiO_2 nanoparticles in the microemulsion increased with time. After 10 h, the intensity and width of the characteristic absorption peak of SiO_2 were similar to that of the SiO_2 nanoparticles after 5 h. Therefore, the formation of SiO_2 nanoparticles in the microemulsion was completed after 5 h.

As shown in Figure S2 (SI), the absorption peaks of SiO_2 become stronger and sharper increasing SiO_2 content. This is because more SiO_2 nanoparticles are formed or the particle size increased. From the TEM images shown in Fig. 2 (TEM micrograph of SiO_2 nanoparticles in the microemulsion at SiO_2 content of 1.0 wt% was listed in Figure S3, SI), more SiO_2 nanoparticles are first formed with increasing reactant content. When the SiO_2 content reached 5.0 wt%, the nanoparticles aggregated (Fig. 2c) to cause the sharpest SiO_2 absorption peaks.

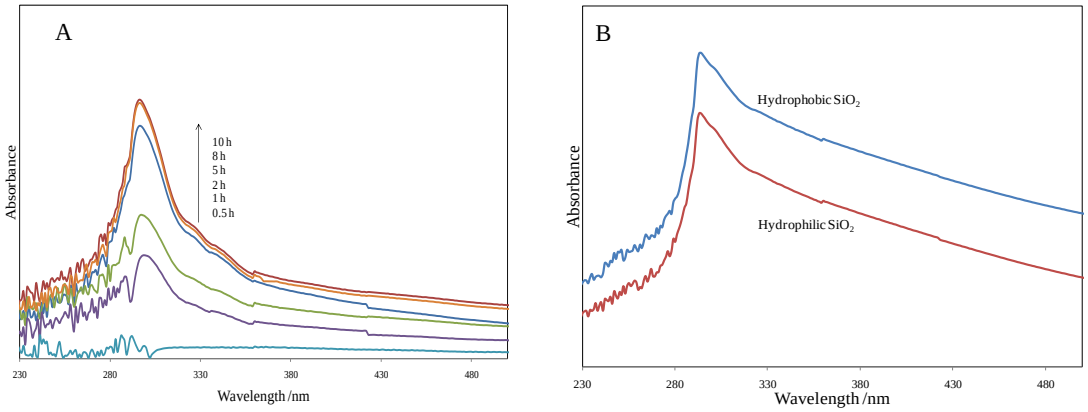

Fig. 1 UV-visible absorption spectra microemulsion and two SiO_2 nanoparticles in the MMA solution(containing 3.0 wt% of SiO_2).

A. Evolution of UV-visible absorption spectra of microemulsion with reaction time; and

B. Two SiO_2 nanoparticles in the MMA solution after treatment in an ultrasonic bath for 1 h.

According to previous studies [24-27], an increased reactant TEOS concentration accelerates the rate of SiO_2 particle formation in the microemulsion to give smaller particles. At a high reactant concentration, too many small SiO_2 particles form. This increases collision and aggregation as shown in Fig. 2c.

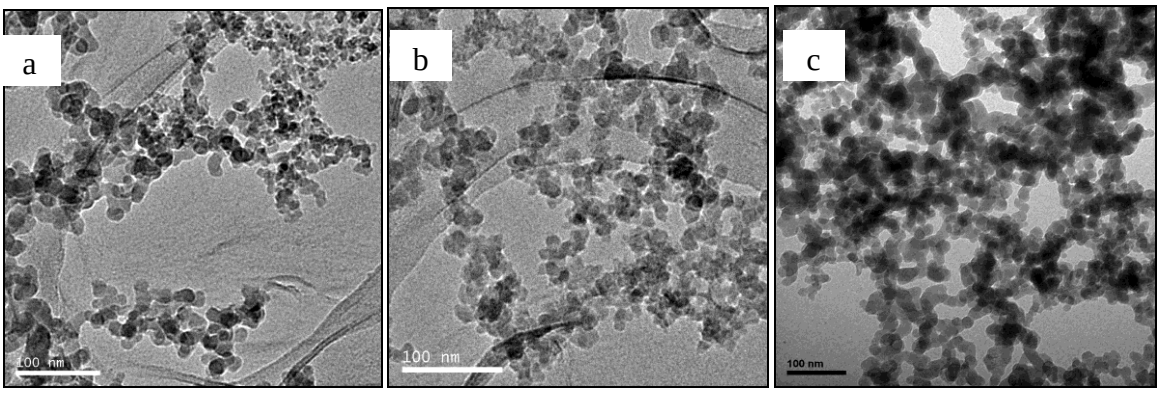

Fig. 2 TEM micrographs of different SiO_2 nanoparticles in the microemulsion at

SiO_2 content of: a. 3.0 wt%; b. 4.0 wt%; and c. 5.0 wt%.

Effect of SiO_2 content on the morphology and performance of the hybrid membranes

SEM Analysis. The SEM images of different hybrid membranes are shown in Fig. 3 (SEM image of the surface of hybrid membrane at SiO_2 content of 1.0 wt% was listed in Figure S4, SI). We found that an increasing number of SiO_2 nanoparticles (white highlights) are formed with increasing SiO_2 content. No marked aggregation of SiO_2 nanoparticles was observed in the SEM images when the SiO_2 content in the hybrid membranes was below 4.0 wt%. At 5.0 wt% SiO_2, large particles were found in the membrane (Fig. 3C). These large particles were caused by the aggregation of SiO_2 that formed in the microemulsion and during polymerization. According to the TEM micrographs (Fig. 2), obvious aggregation of SiO_2 appeared due to the collision between small particles in the microemulsion. In addition, many small particles were prone to form aggregates of SiO_2 during polymerization.

In comparing the morphology of the SiO_2 nanoparticles in the TEM images, the SiO_2 nanoparticles in the hybrid membrane were slightly larger than those before polymerization. According to our former work on the fabrication of hybrid membranes containing AgCl nanoparticles [24-26], the difference between size of SiO_2 particles in TEM morphology and in SEM images was caused by two reasons. First, the SiO_2 nanoparticles in the hybrid membrane were larger than those before polymerization. This increase in size can be ascribed to the coating of the SiO_2 nanoparticles with polymer during polymerization. Otherwise, the interface energy between the surfactant and the particles would change during polymerization and cause the SiO_2 particles to agglutinate.

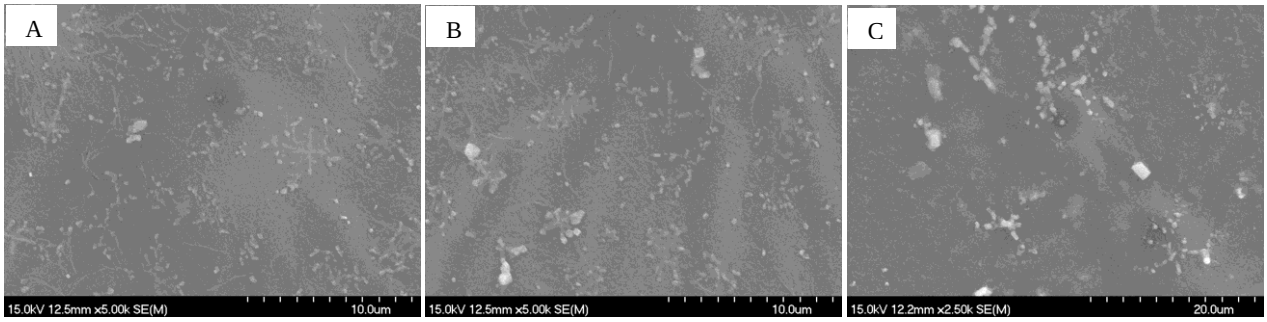

Fig. 3 SEM micrographs of the surface of different SiO_2/PMMA hybrid membranes at SiO_2 content of: A. 3.0 wt%; B. 4.0 wt%; and C. 5.0 wt%.

The measurement of zeta potential values and water contact angles of different hybrid membranes. To explore further the surface property of the hybrid membranes containing different SiO_2 particles, we have also measured the zeta potential values and water contact angles of different membranes, as shown in Fig.4. The zeta potential is used for characterizing the surface electrical properties of the mixed matrix membrane, which is closely related to the quantity and dispersion of SiO_2. More SiO_2 nanoparticles with hydroxyl groups disperse homogenously in the mixed matrix membranes, which led to a larger zeta potential value of the mixed matrix membrane.

It was observed from above figure that the zeta potential for the SiO_2/PMMA membrane at SiO_2 content of 4.0 wt% was the highest among all hybrid membranes in the Figure. That is to say, this hybrid membrane surface showed the highest electrical property, which caused the best surface hydrophilicity as shown in the Figure (the static water contact angles of SiO_2/PMMA membrane at SiO_2 content of 0.0 wt% to 5.0 wt% were 100.5º, 88.4º, 59.8º, 48.7º, 43.5 º, 51.3º, respectively). According to our former work [24-26] and the TEM analysis, more SiO_2 with hydroxyl groups generated in the microemulsion and distributed homogenously in the PMMA polymer matrix, when SiO_2 content was 4.0 wt%. So, the SiO_2/PMMA membrane had the highest electrical property and the

best surface hydrophilicity of the SiO_2/PMMA membrane at SiO_2 content of 4.0 wt%.

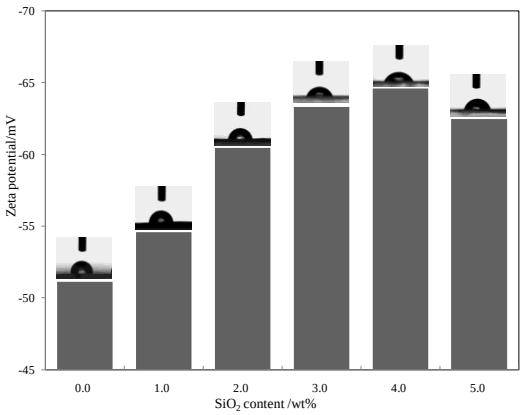

Fig.4 The zeta potential values and water contact angles of different membranes

Separation performance of different hybrid membranes. Figure S5 (SI) shows the permeability measurements using pure CO_2 gas at a wider range of feed pressures. From the figure, the CO_2 permeability of all different SiO_2/PMMA membranes decreases monotonically with the increase of feed pressure, which meant that the plasticization response is not observed. In contrast, the CO_2 permeability of pure PMMA membranes decreases as the feed pressures increases up to 0.840 MPa. When feed pressure is 1.05 Mpa, the permeability increases and indicates that this membrane is plasticized at this feed pressure.

In the permeability measurements using gas mixture at different feed pressures (as shown in Figs. 5 and 6),the CO_2 permeability of all membranes decreases monotonically with the increase of feed pressure. And there is no the plasticization response is not observed. For pure PMMA membrane, the plasticization response is not observed in the permeability measurements using gas mixture at different feed pressures, which might be due to the low content of CO_2 in gas mixture. To clarify this point, we have carried out experiments with mixed gas feeds of high CO_2 content (volume ratio of CO_2/N_2 are 9:1 and 5:5, respectively) for both the pure PMMA and hybrid membranes, as shown in Figures S6 and Figures S7 (SI). From the two figures, it is found that the plasticization response of PMMA membrane is also observed in the permeability measurements using gas mixture with high CO_2 content (volume ratio of CO_2/N_2 are 9:1). However, the plasticization response does not appear, when the CO_2 content in gas mixture decreases to 50% (volume ratio). In contrast, there are also no plasticization responses of hybrid membranes in these two figures. And it confirms the conclusion from Figs. 5 and 6. For hybrid membranes containing SiO_2 nanoparticles, the improvement on plasticization resistance by addition of nanoparticle and the low content of CO_2 in gas mixture both caused the absence of plasticization effects in the mixed gas feed [11]. It can also be observed from Figs. 5 and 6 that both the CO_2 and N_2 permeability decreases a little with increase of feed pressure, which is consistent with the results in many works [29, 30]. It is also found in Figs. 5 and 6 that the CO_2 and N_2 permeability of the hybrid membranes at different feed pressures Both first increased and then decreased with increasing SiO_2 content. Combining with the results in these literature, the improvement on the gas permeability was not only caused by the disruption of the polymer chain packing, but also due to the formation of defects at the interface polymer-filler, when well-distributed SiO_2 inorganic particles with small size added into the polymer matrix. The decrease in the gas permeability was resulted from SiO_2 aggregates in the hybrid membranes, (as shown in Fig. 3C).

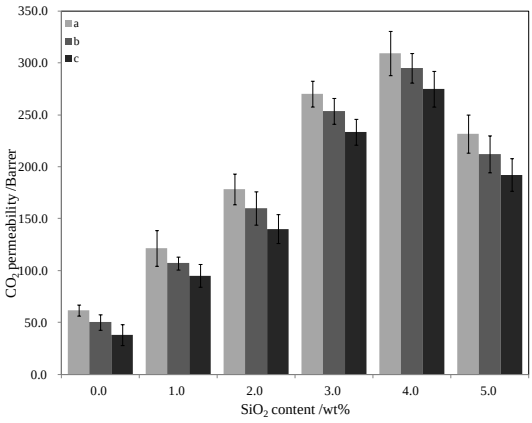

Fig.5 Dependence of CO_2 permeability on the SiO_2 content of the hybrid membranes (Gas mixture)

Feed pressure /MPa: a. 0.105; b. 0.525; c. 1.05

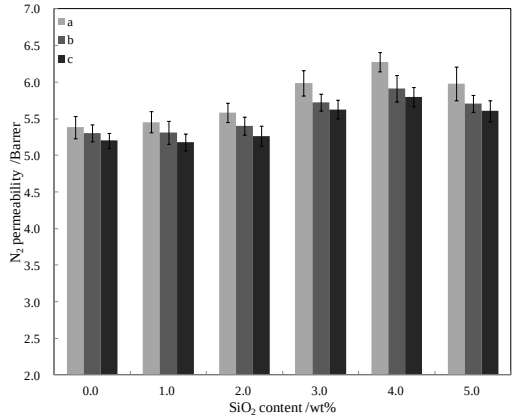

Fig.6 Dependence of N_2 permeability on the SiO_2 content of the hybrid membranes (Gas mixture)

Feed pressure /MPa: a. 0.105; b. 0.525; c. 1.05

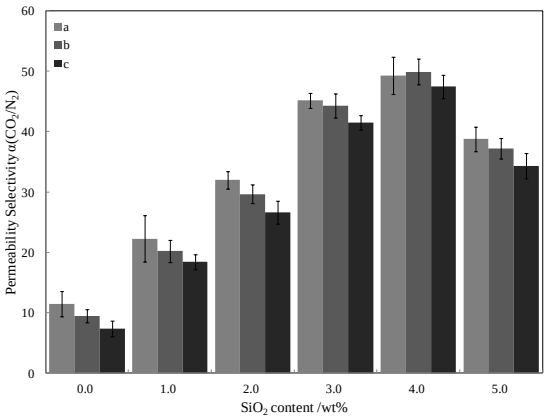

Fig.7 Dependence of permeability selectivity for gas mixture on the SiO_2 content of hybrid membrane

Feed pressure /MPa: a. 0.105; b. 0.525; c. 1.05

Based on the results in Fig. 4, the hydroxyl groups on the surface of well-distributed SiO_2 had a stronger interaction with CO_2 than N_2, which could improve the solubility of polar gas, thus increasing the CO_2/N_2 selectivty [31, 32]. Fig. 7 also shows that the CO_2/N_2 permeability selectivity of the hybrid membranes at first increases with increasing SiO_2 content. The maximum permeability selectivity for the hybrid membranes with 4.0 wt% SiO_2 is about five times that of PMMA membranes without SiO_2. The enhancement on the separation performance caused by SiO_2 addition was more significant than that of MWCNTs on the PU membranes in our former work [28]. However, both the permeability and separation performance of the hybrid membranes decreased when the SiO_2 content reached 5.0 wt%. This is due to SiO_2 aggregates in the hybrid membranes, (as shown in Fig. 3C). The change in the gas permeability and permeability selectivity in also show that the SiO_2 content in the hybrid membranes was a key factor affecting the permeability and separation performance of the membranes.

To confirm this conclusion, we also carried out the gas permeability measurements using a pure gas (CO_2 and N_2). As shown in Figs. 8 and 9, it is also found that the changes in pure CO_2 and N_2 gas permeability of hybrid membranes with SiO_2 content is also similar to that under gas mixture permeation tests.

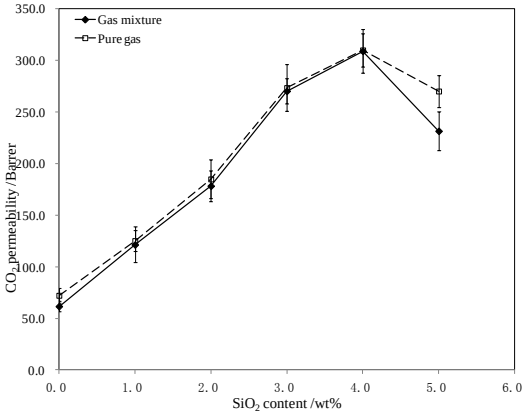

Fig. 8 Dependence of CO_2 permeability on the SiO_2 content of the hybrid membranes

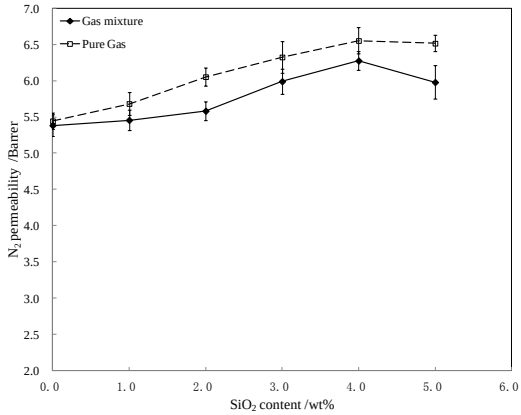

Fig. 9 Dependence of N_2 permeability on the SiO_2 content of the hybrid membranes

RSC Advances

ARTICLE

Fig. 10 shows the changes in the permeability selectivity and ideal selectivity of CO_2/N_2. From the figure, both permeability selectivity and ideal selectivity increases with SiO_2 content in hybrid membranes increasing, due to the addition of more SiO_2 particles with small size and good distribution. It can be seen that the permeability selectivity is higher than the ideal selectivity for all tested membranes, which is attributed to the competitive adsorption in separating gas mixtures [31, 32]. When the SiO_2 content reaches 5.0 wt%, SiO_2 aggregates in the hybrid membranes decreases both the gas permeability and selectivity for CO_2/N_2 of hybrid membranes.

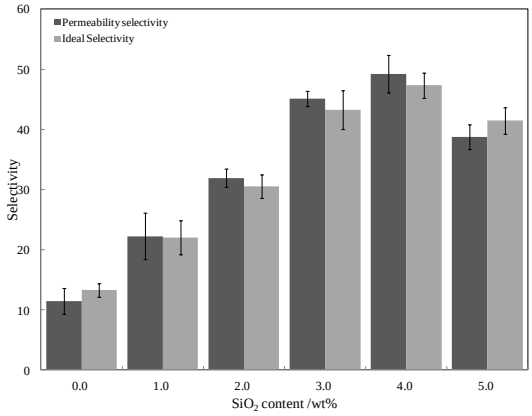

Fig. 10 Dependence of CO_2/N_2 selectivity on the SiO_2 content of hybrid membrane.

Comparison of the hybrid membranes prepared by two methods

For comparison, two commercially available SiO_2 nanoparticles with different surface properties were also used to synthesi - SiO_2/PMMA hybrid membranes by solution polymerization. V - prepared hybrid membranes containing 3.0 and 4.0 wt% of SiO_2 and evaluated their gas performance.

Morphology of SiO_2 in the microemulsion and two commercially available SiO_2 nanoparticles. The TEM images (Fig. 11) show that the size of the two commercially available SiO_2 nanoparticles is similar to our SiO_2 nanoparticles. The SiO_2 nanoparticles dispersed well in the MMA solution because of protection by the water droplets in the reverse microemulsion. Therefore, the SiO_2 nanoparticles formed in the microemulsion show the most homogeneous distribution in the MMA solution among the three SiO_2 nanoparticles after 24 h (Fig. 12). Because MMA is an organic solution, hydrophilic SiO_2 aggregated in the MMA solution. Hydrophobic SiO_2 also slightly precipitated after 24 h.

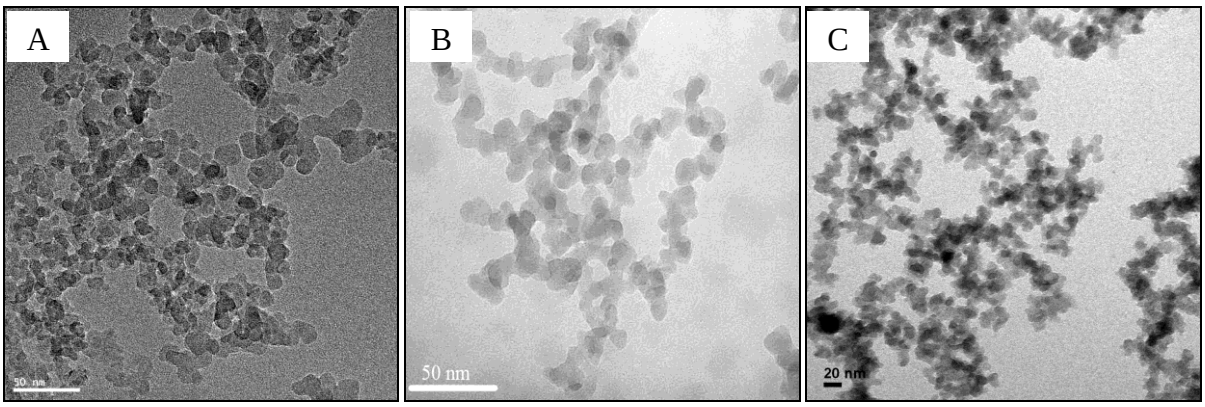

Fig. 11 TEM micrographs of different SiO_2 nanoparticles.

A. Hydrophobic SiO_2; B. Hydrophilic SiO_2; C. SiO_2 nanoparticles formed in the microemulsion. (SiO_2 content was 4.0 wt%)

RSC Advances

ARTICLE

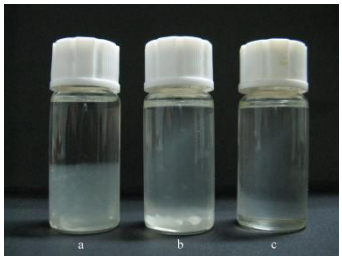

Fig. 12 Photograph of different SiO_2 nanoparticles dispersed in the MMA solution after 24 h.
a. Hydrophobic SiO_2; b. Hydrophilic SiO_2; c. SiO_2 nanoparticles formed in the microemulsion. (SiO_2 content was 4.0 wt%)

FTIR analysis of the SiO_2 nanoparticles. Fig. 13 shows the same characteristic peaks in the FTIR spectra of the three SiO_2 nanoparticles. The band at ~558 cm^{-1} is attributed to the characteristic peak of the aromatic Si–O–Si bending vibration. The bands at 2935 and 2860 cm^{-1} are attributed to the Si–OH and Si–O–Si asymmetric stretching vibrations, respectively. However, the characteristic peaks in the spectra of the three SiO_2 nanoparticles clearly differ in their intensity. The characteristic peaks of hydrophobic SiO_2 were weaker than hydrophilic SiO_2 because of the hydrophobic surface—this results in a better distribution of hydrophobic SiO_2 in the MMA solution.

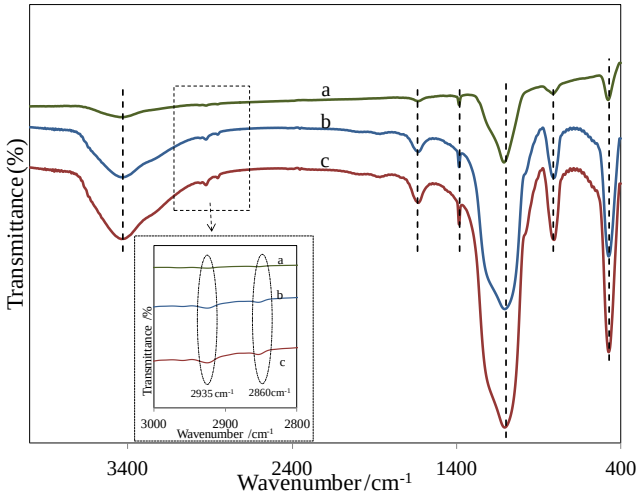

Fig. 13 FTIR spectra of different SiO_2 nanoparticles.
a. Hydrophobic SiO_2; b. Hydrophilic SiO_2; c. SiO_2 nanoparticles formed in the microemulsion. (SiO_2 content was 4.0 wt%)

Moreover, the SiO_2 nanoparticles formed in the microemulsion show their strongest peaks in the FTIR spectrum indicating more hydrophilic groups on their surface. In the reverse microemulsion, both the hydrolysis of TEOS and formation of SiO_2 occurred in the water droplets. Therefore, the surface of the SiO_2 nanoparticles formed in the microemulsion has many hydrophilic groups. The SiO_2 samples with a hydrophilic surface dispersed well in the microemulsion because of protection by water droplets (Fig. 3c).**Morphology of different SiO_2/PMMA hybrid membranes.** Fig. 14 shows clear differences in the morphologies of the three SiO_2/PMMA hybrid membranes. The hydrophobic SiO_2 shows a good affinity with PMMA polymer and is distributed homogeneously in the hybrid membrane. Because of the low affinity between hydrophilic SiO_2 and PMMA polymer materials, the SiO_2 aggregates appeared on the surface of the hybrid membranes containing hydrophilic SiO_2.

Because the surfactant PEO–PPO–PEO (F127) has good compatibility with PMMA [26], the SiO_2 nanoparticles formed in the microemulsion were well protected during MMA polymerization. Therefore, the SiO_2 nanoparticles formed in the microemulsion are homogeneously distributed in the PMMA membrane.

RSC Advances

ARTICLE

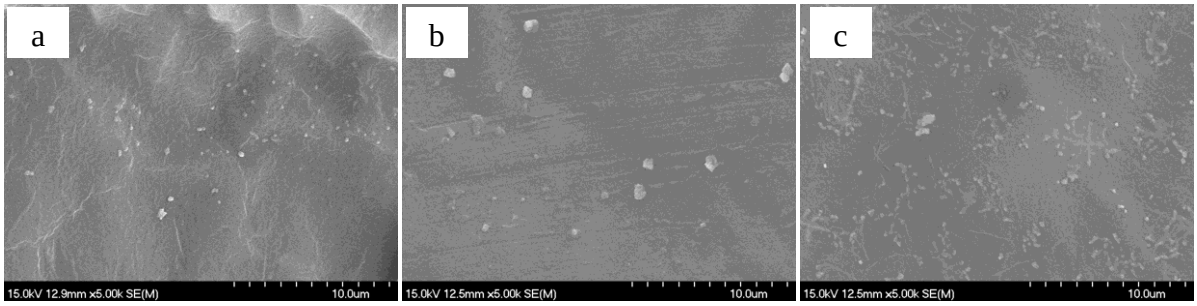

Fig. 14 SEM photographs of different hybrid membranes containing 4.0 wt% of SiO_2.

a. Hydrophobic SiO_2; b. Hydrophilic SiO_2; c. SiO_2 nanoparticles formed in the microemulsion.

Fig. 15 shows the DSC thermograms obtained for the PMMA membrane and the hybrid membranes including three SiO_2 nanoparticles. The endothermic peak at 88°C indicates the glass transition of the PMMA polymer membrane. The glass transition occurs near 120 °C for the other three curves with silica nanoparticles. By the four endothermic peaks, we see that the addition of SiO_2 nanoparticles significantly increased the glass transition temperature (Tg) of the membrane. Another peak near 250 °C for the PMMA membrane suggests membrane decomposition. The addition of SiO_2 nanoparticles also increased the decomposition temperature of the hybrid membranes. That is to say, the hybrid membrane with nanoparticles had a higher thermal stability than membrane without nanoparticles.

There is an obvious difference in the DSC curves of hybrid membranes containing different SiO_2 nanoparticles. Hydrophobic SiO_2 and the SiO_2 nanoparticles prepared by microemulsion showed more homogeneous distribution in the polymer membrane than the hydrophilic SiO_2. Therefore, the hybrid membrane with hydrophilic SiO_2 had the worst thermal stability of the three SiO_2/PMMA hybrid membranes.

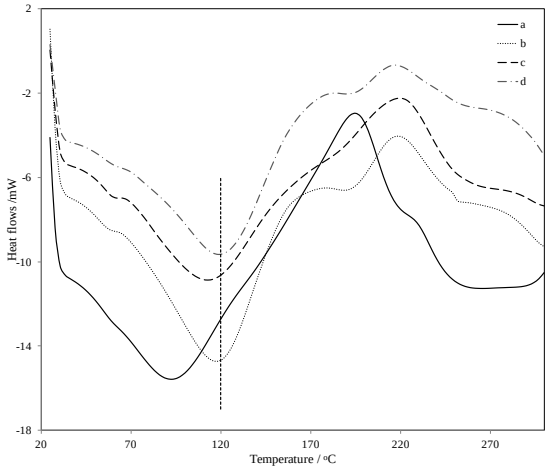

Fig. 15 DSC thermographs for different membranes containing 4.0 wt% of SiO_2.

a. PMMA membrane; b. Hydrophobic SiO_2; c. Hydrophilic SiO_2; d. SiO_2 nanoparticles formed in the microemulsion.

Separation performance of different hybrid membranes. The data in Table 2 show that the addition of different SiO_2 nanoparticles simultaneously enhances the CO_2 permeability and the separation performance of the hybrid membranes, which is consistent with the results in the literature [29, 30]. The different morphologies of the three SiO_2/PMMA hybrid membranes may result in different ga separation performance. The data in Table 2 show that th SiO_2/PMMA hybrid membrane prepared by in situ microemulsi n polymerization has the highest CO_2 permeability and separatio

performance among the three hybrid membranes. The performance of the other two SiO_2/PMMA hybrid membranes is similar despite their very similar morphologies.

Table 2. Gas permeability and separation performance of different hybrid membranes containing different SiO_2 nanoparticles

Membranes	SiO_2 content /wt%	CO_2 permeability /Barrer		N_2 permeability /Barrer		Selectivity	
		Gas mixture	Pure Gas	Gas mixture	Pure Gas	permeability Selectivity	Ideal Selectivity
PMMA	0	61.6	72.2	5.37	5.44	11.5	13.3
H-SiO_2/PMMA[a]	3.0	184.9	188.9	5.88	6.21	31.4	30.4
nonH-SiO_2/PMMA[b]	3.0	186.3	195.3	6.02	6.35	30.9	30.7
M-SiO_2/PMMA	3.0	270.4	273.6	5.85	6.33	46.2	43.2
H-SiO_2/PMMA	4.0	164.9	173.2	5.74	6.11	28.7	28.3
nonH-SiO_2/PMMA	4.0	195.7	211.3	6.31	6.66	31.0	31.7
M-SiO_2/PMMA	4.0	309.2	310.1	6.27	6.55	49.3	47.3

a. H-SiO_2/PMMA means Hydrophilic SiO_2/PMMA; b. nonH-SiO_2/PMMA means Hydrophobic SiO_2/PMMA

From the results in Figs. 14 and 15, SiO_2 nanoparticles in the PMMA polymer matrix prepared by in situ microemulsion polymerization show the most homogenous distribution. Therefore, the resulting hybrid membrane has the highest CO_2 permeability and separation performance among the three hybrid membranes.

In addition, CO_2 is a polar molecule, it interacted strongly with the polar surface of SiO_2 [33, 34]. The hydrophilic SiO_2 has a polar surface but poor distribution in PMMA, whereas the hydrophobic SiO_2 distributed well in PMMA but had a non-polar surface. Therefore, the CO_2 permeability and separation performance of the hydrophilic SiO_2/PMMA membrane was close to that of the hydrophobic SiO_2/PMMA membrane. In situ microemulsion polymerization, we created SiO_2 nanoparticles in water droplets with many hydrophilic groups on their surface suggesting that the nanoparticles had a strongly polar surface. The increase in the surface polarity of SiO_2/PMMA membranes could also enhance the interaction between CO_2 and hybrid membrane, thus leading to the high CO_2 permeability and separation performance [33, 34].

To confirm further the relationship between the surface hydrophilicity of membranes and separation performance of CO_2, we have also provided the zeta potential values and water contact angles of containing different SiO_2 nanoparticles, as shown in Figure S8 (SI). From the figure, it is found that addition of nonH-SiO_2 (R972) causes a smaller zeta potential value of membranes and increases the surface hydropholic surface, which is content with the results in the literatures [35]. When SiO_2 with hydrophilic surface added (H-SiO_2), the zeta potential values of hybrid membranes increases and the water contact angles of hybrid membranes decrease. More SiO_2 nanoparticles with hydroxyl groups disperse homogenously in the mixed matrix membranes, which led to a larger zeta potential value of the mixed matrix membrane. It is also found from the figure that SiO_2/PMMA hybrid membranes via in-situ microemulsion polymerization have the largest zeta potential values and the smallest water contact angles under the same addition content of SiO_2, due to the strongest polar surface of SiO_2 nanoparticles formed in reverse microemulsion. These all cause the high CO_2 permeability and separation performance.

Conclusions

Small SiO_2 nanoparticles were formed with a reverse microemulsion using PEO–PPO–PEO (F127) as the surfactant and MMA as the oil phase. The nanoparticles were formed after 1 h and completed after 5 h. Then, SiO_2/PMMA hybrid membranes with different SiO_2 contents were prepared by in situ microemulsion polymerization. Both the gas permeability and the separation performance of the hybrid membranes first increased and then decreased with increasing SiO_2 content. When SiO_2 reached 4.0 wt%, the permeability selectivity of the hybrid membranes for CO_2/N_2 gas mixtures was maximal. At higher loading levels (5.0 wt%), the SiO_2 aggregated and gas permeability and separation decreased.

For comparison, two commercial SiO_2 nanoparticles were also used to synthesize SiO_2/PMMA hybrid membranes by solution

polymerization. Due to the protection by the microemulsion, the SiO_2 nanoparticles formed in the microemulsion distributed well in the MMA solution and PMMA matrix polymer. This led to high thermal stability of the hybrid membranes. In addition, the surface of the SiO_2 nanoparticles formed in the water droplets contained many hydrophilic groups. Therefore, the SiO_2/PMMA hybrid membrane prepared by in situ microemulsion polymerization had a higher CO_2 permeability and separation performance than hybrid membranes containing two commercial SiO_2 nanoparticles.

Acknowledgements

The financial support from the National Science Foundation of China Grants (Contract 21376218, 21076190 and 51103130) and the Natural Science Foundation of Zhejiang Province (Contract LY14B060001) is gratefully acknowledged.

Notes and references

1 G. Centi and S. Perathoner, ChemSusChem, 2010, **3**, 195−208.

2 L. Hammarstrom and S. Hammes-Schiffer, *Acc. Chem. Res.* 2009, **42**, 1859−1860.

3 F. H. Akhtar, R. W. Pinder, D. H. Loughlin and D. K. Henze, *Environ. Sci. Technol.* 2013, **47**, 12011–12019.

4 R. Xing and W. W. S. Ho, *J. Membr. Sci.* 2011, **367**, 91–102.

5 X. Ren, J. Ren, and M. Deng, *Sep. Purif. Technol.* 2012, **89**, 1–8.

6 L. Shao, B. T. Low, T. S. Chung and A. R. Greenberg, *J. Membr. Sci.* 2009, **327**, 18–31.

7 R. W. Baker, *Ind. Eng. Chem. Res.* 2002, **41**, 1393–1411.

8 D. Bastani, N. Esmaeili and M. Asadollahi, *J. Ind. Eng. Chem.* 2013, **19**, 375–393.

9 C. J. Cornelius and E. Marand, *J. Membr. Sci.* 2002, **202**, 97–118.

10 Y. Xiao, B. T. Low, S. S. Hosseini, T. S. Chung and D. R. Paul, *Prog. Polym. Sci.* 2009, **34**, 561–580.

11 M. S. Boroglu and M. A. Gurkaynak, *Polym. Adv. Technol*. 2011, **22**, 545–553.

12 T. Wang and D. H. Yan, *Adv. Colloid Interf. Sci.* 2014, **7**, 332–356.

13 A. G. Kannan, N. R. Choudhury and N. K. Dutta, *Polymer* 2014, **55**, 5132–5139.

14 P. S. Goh, A. F. Ismail, S. M. Sanip, B. C. Ng and M. Aziz, *Sep. Purif. Technol.* 2011, **81**, 243–264.

15 M. C. Ferrari, M. Galizia, M. G. De Angelis and G. C. Sarti, *Ind. Eng. Chem. Res.* 2011, **49**, 11920–11935.

16 K. Kusakabe, K. Ichiki, J. Hayashi, H. Maeda and S. *J.* Morooka, *Membr. Sci.* 1996, **115**, 65–75.

17 T. C. Merkel, Z. He, I. Pinnau, B. D. Freeman, P. Meakin and A. J. Hill, *Macromolecules* 2003, **36**, 6844–6855.

18 T. C. Merkel, B. D. Freeman, R. J. Spontak, Z. He, I. Pinnau, P. Meakin and A. J. Hill, *Chem. Mater*. 2003, **15**, 109–123.

19 L. M. Jin, S. L. Yu, W. X. Shi, X. S. Yi, N. Sun, Y. L. Ge and C. Ma, *Polymer* 2012, **53**, 5295–5303.

20 B. N. Nair, W. J. Elferink, K. Keizer and H. Verweij, *J. Colloid Interf. Sci*. 1996, **178**, 565–570.

21 C. R. Silva and C. Airoldi, *J. Colloid Interf. Sci.* 1997, **195**, 381–387.

22 C. H. Lau, S. L. Liu, D. R. Paul, J. Z. Xia, Y. C. Jean, H. M. Chen, L. Shao and T. S. Chung, *Adv. Energy Mater.* 2011, **1**, 634–642.

23 J. Eastoe, M. J. Hollamby and L. Hudson, *Adv. Colloid Interf. Sci.* 2006, **128–130**, 5–15.

24 L. G. Wu, T. Wang and Z. Jiang, *J. Membr. Sci.* 2013, **429**, 95–102.

25 L. G. Wu, J. N. Shen, C. H. Du, T. Wang, Y. Teng and B. V. Brugg, *Sep. Purif. Technol.* 2013, **114**, 117–125.

26 L. G. Wu, T. Wang and W. Xiang, *Composites Sci. Technol.* 2013, **80**, 8–15.

27 M. Lu, Y.Y. Zhou, Y.C. Zhu, J. Lian, T.H. Lin, T. Wang, L.G. Wu and T. Fang, *Adv. Mater. Res.* 2013, **750-752**, 1897–1900.

28 T. Wang, J. N. Shen, L. G. Wu, B. V. Bruggen, *J. Membr. Sci.* 2014, **466**, 338–347.

29 S. Matteucci, V. A. Kusuma, S. Swinnea, and B. D. Freeman, *Polymer*, 2008, **49**, 757–773.

30 D. F. Sanders, R. L. Guo, Z. P. Smith, K. A. Stevens, Q. Liu, J. E. McGrath, D. R. Paul, and B. D. Freeman, *J. Membr. Sci.* 2014, **463**, 73–81.

31 J.H. Kim and Y.M.Lee, *J. Membr. Sci.* 2001, **193**, 209–225.

32 M. Wang, Z. Wang , J. Wang, Y. Zhu and S. Wang, *Energy Environ. Sci.* 2011, **4**, 3955–3959.

33 R. Swaidan, B. Ghanem, E. Litwiller and I. Pinnau, *J. Membr. Sci.* 2015, **475,** 571–581.

34 J. D. Wind, D. R. Paul and W. J. Koros, *J. Membr. Sci.* 2004, **228**, 227–236.

35 B. N. Sahoo and B. Kandasubramanian, *RSC Adv.* 2014, **4**, 22053–22093.